Sensors and Actuators B 186 (2013) 205–211

Contents lists available at SciVerse ScienceDirect

Sensors and Actuators B: Chemical

journal homepage: www.elsevier.com/locate/snb

Incident-angle dependence of fluorescence enhancement and biomarker immunoassay on gold nanohole array

Yi Wang[a,*,1], Lin Wu[b,1], Xiaodong Zhou[c,**], Ten It Wong[c], Jinling Zhang[a], Ping Bai[b], Er Ping Li[b], Bo Liedberg[a]

[a] Centre for Biomimetic Sensor Science, Nanyang Technological University, 50 Nanyang Drive, Research Techno Plaza 6th Storey, XFrontiers Block, Singapore 637553, Singapore
[b] Electronics and Photonics Department, Institute of High Performance Computing, Agency for Science, Technology, and Research (A*STAR), 1 Fusionopolis Way, Singapore 138632, Singapore
[c] Institute of Materials Research and Engineering, Agency for Science, Technology and Research (A*STAR), 3 Research Link, Singapore 117602, Singapore

ARTICLE INFO

Article history:
Received 29 March 2013
Received in revised form 29 May 2013
Accepted 4 June 2013
Available online 14 June 2013

Keywords:
Nanohole array
Surface plasmon
Fluorescence enhancement
Biosensors

ABSTRACT

We theoretically and experimentally investigate the influence of the incident angle of illumination on the fluorescence enhancement for two kinds of gold nanohole arrays – a gold nanohole array on glass substrate (Au-hole array), and a gold coated photoresist nanohole array (Au/PR-hole array). Our simulations show that the absorption spectra for the Au/PR-hole array vary substantially with angle of incidence, whereas the corresponding spectra for the Au-hole array are marginally affected. The experimental results reveal fluorescence enhancement up to 14 and 12 times for the Au-hole array at an incident angle of 70° and the Au/PR-hole array at an incident angle of 20°, respectively. Moreover, a model sandwich immunoassay for the detection of prostate specific antigen (PSA) shows about 3-fold higher sensitivity on Au/PR-hole array as compared to planar gold at 70°. To the best of our knowledge this is the first investigation reporting on the relationship between the incident angle and the fluorescence enhancement on gold nanohole arrays. Our findings provide a solid foundation for designing a highly efficient fluorescence detection system with oblique angular illumination.

1. Introduction

Gold nanohole arrays have been extensively utilized in label-free [1–6] and plasmon-enhanced fluorescence biosensing [7–13]. In the research field of plasmon enhanced fluorescence, several experimental factors have been identified as critical for achieving maximum fluorescence enhancement. First, an optimal distance between the fluorescent dyes and the metallic surface needs to be considered to minimize fluorescence quenching [14,15]. Second, the spectral overlap between the fluorophore excitation spectrum and the plasmon absorption spectrum of the nanostructures is required for high fluorescence enhancement [16]. Third, periodic nanostructures such as gold nanohole arrays typically provide sharper plasmonic absorption and thus higher fluorescence enhancement than randomly distributed nanostructures [11]. Fourth, the fabrication parameters of a gold nanohole array including the hole size, pitch and thickness can be tuned to optimize the fluorescence enhancement [17]. Thus, proper design of the gold nanohole array is crucial for obtaining maximum fluorescence enhancement. Furthermore, it has been demonstrated that the illumination from the front or back side of the nanohole array does not affect the plasmonic wavelength. However, front side illumination is favorable as it provides a stronger coupling between the incident electromagnetic field and the nanostructure as compared to back side illumination [18].

The combination of fluorescence excitation and a dark-field microscopy is considered to be one of the most sensitive methods for fluorescence detection as it provides lower background emission, higher fluorescence signal-to-noise ratio and hence higher sensitivity as compared to normal fluorescence spectroscopy [16]. For instance, confocal fluorescence microscopy has been implemented for the detection [19] and tracking [20] of single fluorescent molecules on nanoantennas, fluorescence microscopic imaging on 1D and 2D grating structures [21,22], and femtomolar sensitivity detection of biomarkers on a rough gold surfaces [23]. In dark-field microscopy such as the ones used in Refs. [21–23], the sample is peripherally illuminated at large oblique angles. Such an illumination may influence the fluorescence enhancement because the strength and localization of plasmonic field at the metallic

* Corresponding author. Tel.: +65 65927948.
** Corresponding author. Tel: +65 68727522.
E-mail addresses: yiwang@ntu.edu.sg (Y. Wang), donna-zhou@imre.a-star.edu.sg (X. Zhou).
[1] These authors contributed equally to this paper.

0925-4005/$ – see front matter © 2013 Elsevier B.V. All rights reserved.
http://dx.doi.org/10.1016/j.snb.2013.06.018

nanostructures may depend on the light incident angle [24]. Unfortunately, the dependence of the incident angle on the fluorescence enhancement utilizing surface plasmon resonance excitation of nanohole arrays has not been thoroughly investigated in literature, although this information is crucial for the design of nanostructures and optical system for optimized fluorescence excitation.

In this work, we have fabricated two different gold nanohole arrays including a gold nanohole array on glass substrate (Au-hole array), and a gold coated photoresist nanohole array (Au/PR-hole array). The electromagnetic field distribution and the angular-dependent maximum field enhancement on these Au nanohole arrays are investigated by utilizing finite element method (FEM) simulation. The angular-dependent fluorescence enhancements of the Au nanohole arrays are measured in a fluorescence spectrometer and compared with experiments on glass. Finally, a model sandwich immunoassay for the detection of prostate specific antigen (PSA) is performed on the Au/PR-hole array and compared with experiments undertaken on a planar gold substrate.

2. Simulations and experiments

2.1. Simulation method

In the simulation, three-dimensional Maxwell's equations were solved using the finite element method (COMSOL Multiphysics). The wavelength-dependent dielectric function of gold was taken from the Palik handbook [25]. The refractive indices for air, water, glass, and UV curable photoresist were 1, 1.33, 1.52, and 1.422, respectively. A unit cell consisting of one nanohole was simulated. At the sides of the unit cell, Floquet periodic boundary condition was assumed in order to obtain the optical response of the whole nanohole array upon illumination at different angle of incidence. An obliquely-incident linearly-polarized white light source (400–900 nm) was used. As the incident light wave strikes a metal nanohole array, its power will either be absorbed, reflected, or transmitted through the structure. The absorbed power was computed through the volume integration of the resistive heating in the gold nanoparticles, and the reflected or transmitted power was calculated through the surface integration of the far-field power flow [17,18]. In addition, the near-field information at the resonant wavelengths in which we are interested can be directly obtained from the simulations.

2.2. Gold nanohole fabrication

Mass fabrication of the gold nanohole structures was obtained by nanoimprint lithography with a nickel mold [26]. The Au-hole array was fabricated with pitch $P = 400$ nm, diameter $D = 140$ nm, and thickness $T = 50$ nm (5 nm chromium and 45 nm of gold), while the Au/PR-hole array was obtained by coating 50 nm gold film (5 nm chromium and 45 nm of gold) on a photoresist

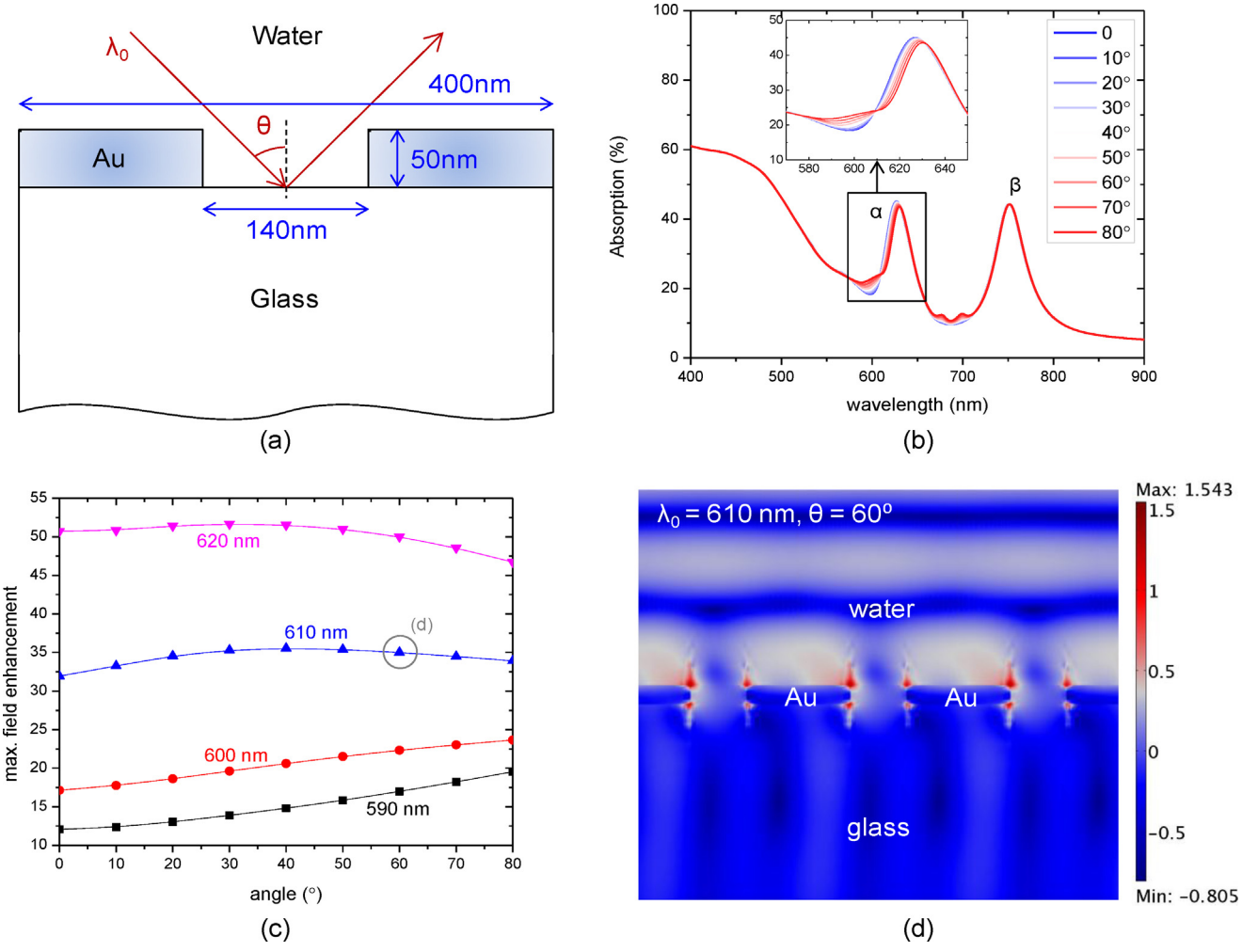

Fig. 1. (a) The simulation model of an Au-hole array ($P = 400$ nm, $D = 140$ nm, $T = 50$ nm) on glass at an incident angle of θ. (b) The absorption spectra of the Au-hole array simulated in water at various incident angles. (c) The simulated maximum field enhancement versus the incident angle at the wavelengths of 590, 600, 610, and 620 nm. (c) The field distribution of Au-hole array at the illumination wavelength of 610 nm and the incident angle of 60°.

nanohole array with $P = 400$ nm, $D = 140$ nm. Briefly, the Au-hole arrays were fabricated with an electroplated nickel mold (with nanoholes structure), which was used to nanoimprint the UV curable photoresist layer (mr-UVCur21-300 nm from Micro Resist Technology, GmbH). The photoresist was then treated with reactive ion etching (RIE) to etch the photoresist down to the glass substrate. Afterwards, 5 nm of chromium and 45 nm thick of gold were deposited, and the photoresist was lifted-off by plasma etching and subsequent rinsing with acetone and isopropyl alcohol [26]. Similarly, the Au/PR-hole array was fabricated with another nickel mold (with nanopillars) which was imprinted on a photoresist and treated with RIE before the gold film evaporation.

2.3. Measurement of UV–vis and fluorescence spectra

The UV–vis transmission spectra of gold nanohole arrays were measured with a UV–vis spectrometer (Lambda 35, PerkinElmer). A black paper with a 2 mm diameter hole was attached to the gold nanohole array to allow the light passing exclusively through the nanohole structure.

The prostate specific antigen (PSA) detection antibodies (from SunnyLab of SCIPAC Ltd) were labeled with Alexa Fluor® 647 (Invitrogen, Singapore) according to the manual of the protein labeling kit (A20173). Afterwards, 5 μl of 6.3 μM Alexa 647 labeled PSA antibody (Ab-AF647) in PBS was dropped on the bare glass, gold film, Au-hole and Au/PR-hole array substrates, respectively. A dye spot with diameter of 3.5 mm was formed on the substrate after drying at room temperature. The fluorescence spectra of the substrates were measured with a fluorescence spectrophotometer (Fluolog, Horiba).

2.4. Surface modification and immunoassay on gold nanohole array

To immobilize capture antibody (c-Ab) on the surface, the gold nanohole array and planar gold film substrates were first modified with thiol-COOH by incubating the substrate in a 1 mM PEG7 thiol acid (thiol-COOH, Product #37156-0795 from Polypure AS, Norway) ethanol solution overnight. The carboxylic acid groups on the substrate were activated with freshly prepared EDC (37.5 mg/ml) and NHC (11.5 mg/ml) water solution. The capturing antibody (c-Ab) was immobilized on the surface by incubating the substrate in 50 μg/ml c-Ab buffer solution for 2 h, followed by incubation with 1 M ethanolamine to deactivate the unreacted carboxylic acid groups.

For the sandwich immunoassay of PSA, phosphate-buffered saline with Tween-20 (PBST) buffer spiked with different

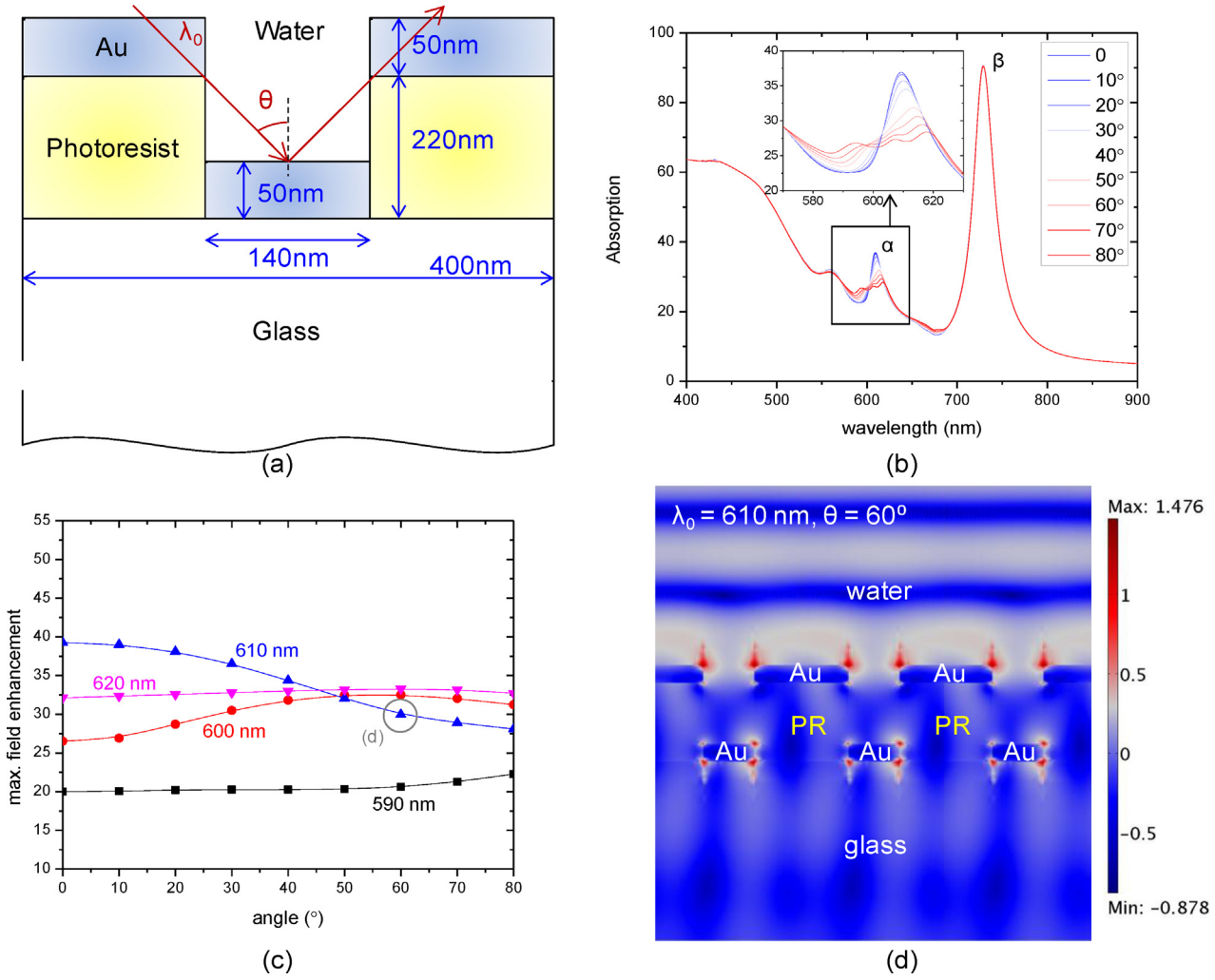

Fig. 2. (a) The simulation model of an Au/PR-hole array with a 50 nm of gold coated on a 220 nm thick photoresist nanohole array ($P = 400$ nm, $D = 140$ nm), and (b) the simulated absorption spectra of Au/PR-hole array in water at various incident angles. (c) Maximum field enhancement versus the incident angle at the wavelengths of 590, 600, 610, and 620 nm. (d) The field distribution of Au/PR-hole at the illumination wavelength of 610 nm and the incident angle of 60°.

concentrations of PSA were incubated on the substrate with a flow-cell for 30 min. After 2 min rinsing with PBST buffer, 10 nM detection antibody, Ab-AF647, was pumped into the flow-cell (volume of 100 μl) and incubated for 20 min. The fluorescence spectra were measured with the fluorescence spectrometer with the light passing through the glass flow-cell and shedding at the surface of the sensor substrate at an excitation wavelength of 610 nm and an incident angle of 70°.

3. Results and discussions

3.1. Simulations for Au-hole array

It is reported that maximum fluorescence enhancement can be achieved through matching the absorption spectrum of the nanostructure with the excitation spectrum of the fluorescence dye [16]. In addition, based on our previous simulation on gold nanohole arrays [17], we designed and fabricated the Au-hole array with $P = 400$ nm, $D = 140$ nm, and $T = 50$ nm (Fig. 1a) as a suitable nanostructure for fluorescence excitation of Alexa 647. At normal incidence, the simulated absorption spectra of the gold nanohole array in water medium (Fig. 1b) show two peaks at around 626 nm and 750 nm, which are related to the α and β plasmon modes, respectively. Previous work [18] has reported that the α mode is associated with the field localized on the top rims of the gold nanoholes (see Fig. 1d), while the β mode is mainly related to the field located at the bottom rims of the gold nanoholes.

The simulated spectra in Fig. 1b indicate that variations of the incident angle from 0° to 80° cause a small ~5 nm red-shift of the α mode, whereas no shift is observed for the β mode. The maximum field enhancements for the incident wavelengths of 590, 600, 610 and 620 nm (Fig. 1c) also indicate small variations upon the changing the incident angle. For example, a maximum field enhancement of 37 is obtained at the wavelength of 610 nm with a variation within 10% for all incident angles. A field intensity independent of the incident angle is desired to minimize the variations of fluorescence enhancement in a fluorescence detection system, such as fluorescence microscopy, where the exciting illumination is distributed over a fairly broad range of incident angles. A representative field distribution at the illumination wavelength of 610 nm and incident angle of 60° (Fig. 1d) indicate that the field penetrates into the water at a depth of ~40 nm. This field penetration depth of the nanohole substrate is suitable for fluorescence enhancement, because it is longer than the typical Förster resonance energy transfer (FRET) distance of ~10 nm [27].

3.2. Simulations for Au/PR-nanohole array

The other gold nanohole structure (Fig. 2a), where a layer of gold is evaporated on top of a photoresist nanohole array (Au/PR-hole array, with $P = 400$ nm, $D = 140$ nm, and $T = 50$ nm), also has been utilized for localized surface plasmon (LSPR) biosensing [28]. Different from Fig. 1b, in the presence of the 220 nm thick photoresist, the α and β modes of the Au/PR-hole array appear blue-shifted to $\lambda_\alpha = 608$ nm and $\lambda_\beta = 726$ nm at normal incidence because of the lower refractive index of the photoresist as compared to glass (Fig. 2b). The absorption peak of the α mode is more sensitive to changes in the incident angle on Au/PR-hole array (Fig. 2b), as compared with the Au-hole array. As the incident angle increases, the peak associated with the α mode is broadened and slightly

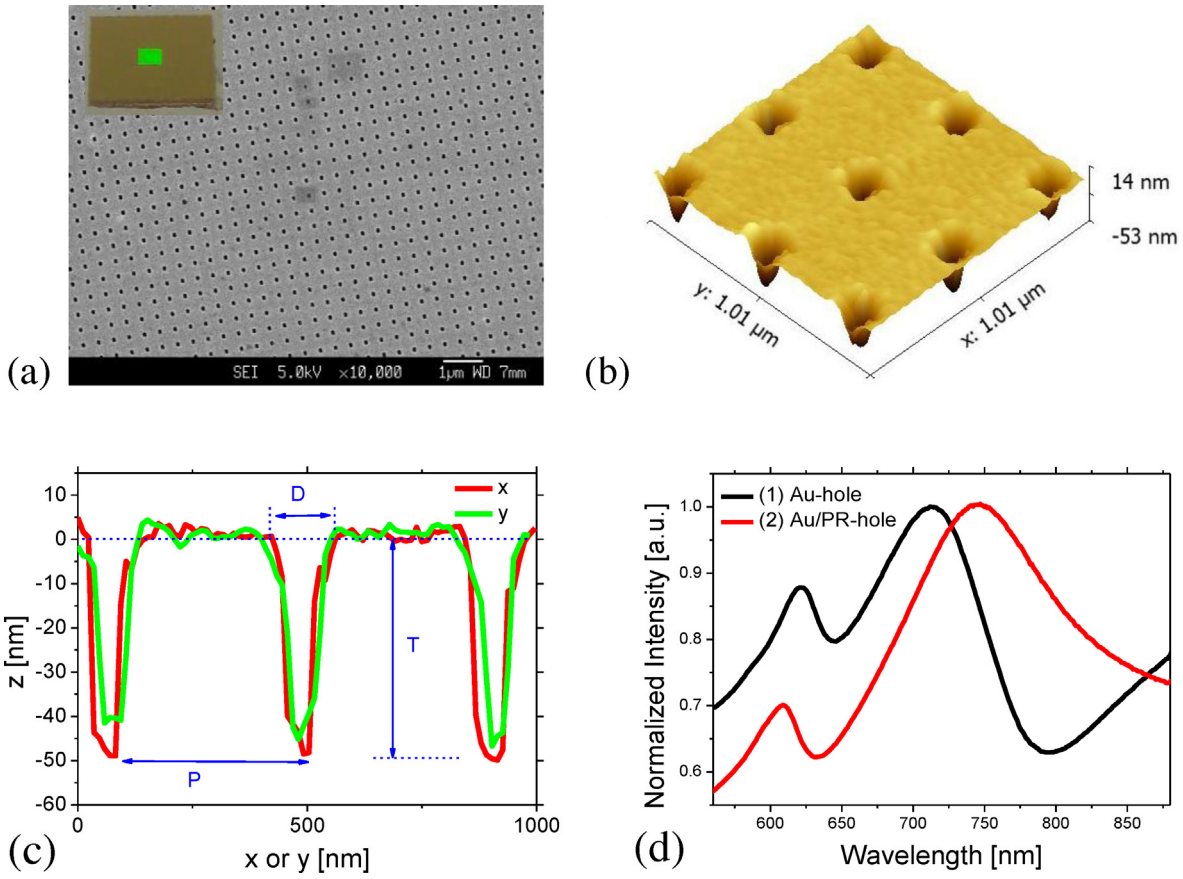

Fig. 3. SEM (a) and AFM images (b) of Au-hole array with 50 nm thick gold. Insert of (a) is a photograph of a 2 cm × 2 cm glass substrate with Au-hole array at the center. (c) The cross-section profile of Au-hole array in (b) at x and y-axis shows $P = 400$ nm, $D = 140$ nm, $T = 50$ nm. (d) UV–vis spectra of (1) Au-hole array with $T = 50$ nm and (2) Au/PR-hole array with 50 nm of gold coated on 220 nm thick photoresist nanohole array in contact with water.

red-shifted and appears with reduced intensity, and it further splits into three separate features (Fig. 2b). This is probably due to the presence of two more interfaces (glass/photoresist, photoresist/Au), which also may contribute the appearance of an additional peak at around 575 nm.

The angle dependent field distribution as plotted in Fig. 2c indicate that the maximum field enhancements at the wavelengths of 600 and 610 nm are more dependent on the light incidence angle than those at 590 and 620 nm, with a variation up to 33% over the entire angular span. Our simulations further indicate that the field distribution for the wavelengths of 590, 600, 610, and 620 nm at different angles are the same, and resembles the one shown for $\lambda_o = 610$ nm and $\theta = 60^\circ$ in Fig. 2d. It is furthermore noticed that the plasmonic hotspots at the top rims of the gold nanoholes provide the highest field enhancement and potentially also the highest fluorescence enhancement.

3.3. Characterizations of Au nanohole array

The Au-hole arrays fabricated at a high throughput on a 2 cm × 2 cm glass substrate with a 2 mm × 2 mm nanohole structure at the center, displayed a diffraction pattern in green color (Fig. 3a). For these kinds of gold nanohole arrays, the yield is nearly 100% as concluded by visual inspection of the diffraction pattern by the naked eye and by SEM imaging (Fig. 3a). Atomic force microscope (AFM) was employed to investigate the size of the nanoholes and their distribution as shown in Fig. 3b. The cross-section profile in Fig. 3c reveals that the fabricated Au-hole array has $P = 400$ nm, $D = 140$ nm and $T = 50$ nm.

The UV–vis spectra of the Au-hole and Au/PR-hole arrays were measured in water, Fig. 3d. The spectrum of the Au-hole array shows two peaks at $\lambda_1 = 621$ nm and $\lambda_2 = 716$ nm which are associated with α and β plasmon modes, respectively. λ_2 in our experiments is smaller than the one simulated at normal incidence, probably because (1) the nanohole size and shape differs slightly from the model used in the simulations, and (2) the 5 nm Cr adhesive layer is not considered in our simulations (note that the β mode is associated with the electromagnetic field on the glass side [18]). Similarly, the Au/PR-hole array with photoresist shows two peaks at $\lambda_1 = 609$ nm and $\lambda_2 = 745$ nm in water. The first peak is comparable with the simulated spectra for α mode plasmon at 608 nm. More importantly, it is noticed that the spectra of the gold nanohole arrays after coated with Ab-AF647 revealed the first peak around 610 nm (measured in air). Therefore, in the following fluorescence measurement, incident light at a wavelength of 610 nm was employed for the excitation of fluorescence.

3.4. Fluorescence enhancement and immunoassay

The angular fluorescence measurements were carried out by rotating the substrate to vary the incident angle θ. The detector is mounted perpendicular to the incident light beam (Fig. 4a). The

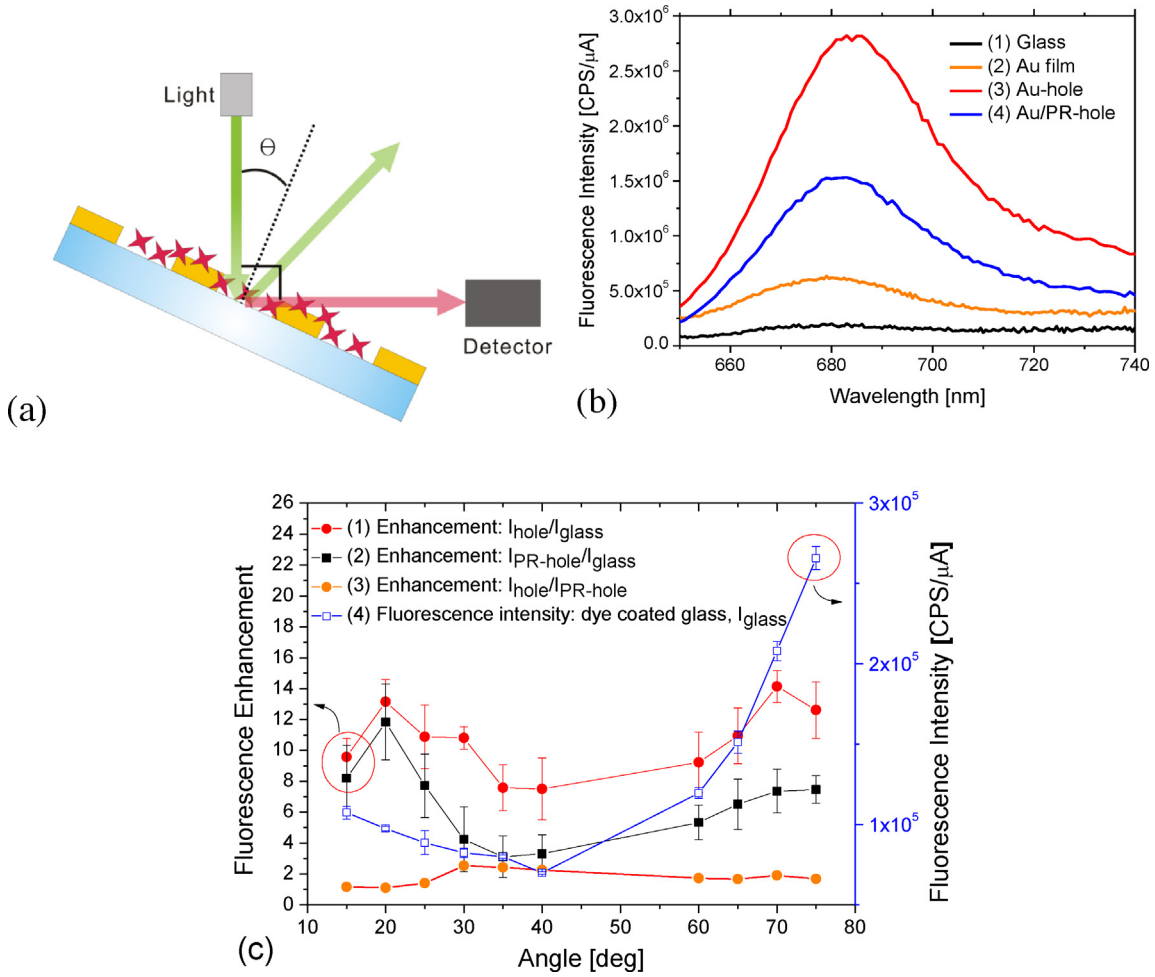

Fig. 4. (a) A scheme presenting the fluorescence measurement on gold nanohole array in a fluorescence spectrophotometer, with light incident angle θ adjusted by rotating the substrate. (b) The fluorescence spectra measured on (1) glass, (2) Au film, (3) Au-hole array and (4) Au/PR-hole array at $\theta = 70^\circ$ and excitation wavelength of $\lambda = 610$ nm. (c) The angular dependent fluorescence enhancement on (1) Au-hole (I_{hole}/I_{glass}), and (2) Au/PR-hole ($I_{PR\text{-}hole}/I_{glass}$), and (3) $I_{hole}/I_{PR\text{-}hole}$ calculated based on (4) the corresponding fluorescence intensity on bare glass substrate I_{glass}.

fluorescence spectra for dye-coated bare glass, planar gold film, Au-hole array and Au/PR-hole array substrates are shown in Fig. 4b for an excitation wavelength of $\lambda_o = 610$ nm (2 nm slit width) and $\theta = 70^\circ$. The fluorescence intensities are enhanced by a factor of 14 and 8 by the Au-hole and Au/PR-hole array, respectively, when compared to that of a bare glass substrate. The flat gold film also shows about 3-fold higher fluorescence intensity than that on glass. The results from the simulations, Figs. 1c and 2c, predict maximum field enhancements at $\lambda_o = 610$ nm and $\theta = 70^\circ$ around 35 and 28 for Au-hole and Au/PR-hole array, respectively. This overestimation by the simulations is expected, as the measurements report the average enhancement rather than the maximum achievable enhancements.

The angular dependent fluorescence enhancements on Au-hole and Au/PR-hole array (Fig. 4c) indicate a maximum fluorescence enhancement of 14 and 12 at the incident angle of 70° and 20°, respectively. The fluorescence enhancement (f) was calculated based on the equation $f = I_{hole}N_{glass}/I_{glass}N_{hole}$, where I_{hole} and I_{glass} are the measured fluorescence intensities, N_{hole} and N_{glass} are the number of dye molecules coated on the Au nanohole array and glass substrates, respectively. In this study, the amount of dye molecules dropped on the glass and nanohole substrates are the same, i.e. $N_{hole} = N_{glass}$. The fluorescence intensity of the dye on bare glass also depends on the incident angle with a minimum occurring at 40° (Fig. 4c). This dependence is attributed to the scattering and background signal from the substrate which is taken into account when calculating the fluorescence enhancement. The average enhancements for the Au-hole and Au/PR-hole arrays at various incident angles are $f = 10.7 \pm 2.2$ and $f = 6.5 \pm 2.6$, respectively, suggesting that the Au/hole array provides on average a factor ~2 higher fluorescence enhancement than the Au/PR-hole array. Moreover, the angular fluorescence enhancement for the Au-hole arrays shows less variation $f = 14$–8 as compared to the Au/PR-hole array $f = 12$–3. The angular-dependent fluorescence measurements are comparable to the simulated trends at the wavelength of 610 nm in Figs. 1c and 2c. The discrepancy between experiments and simulations is attributed to scattering and potentially also fluorescence quenching on the gold nanohole surface. The lower fluorescence enhancement on Au/PR-hole as compared with the Au-hole array might also be ascribed to increased fluorescence quenching (such as FRET) occurring in the deep hole of Au/PR-hole substrate. In conclusion, our findings suggest that the fluorescence enhancement on gold nanohole array can be readily tuned by varying the angle of incident light and the design of the nanostructures.

To demonstrate plasmon enhanced fluorescence for biosensing, we employed a sandwich assay for the detection of PSA on Au film and Au/PR-hole array substrates at $\lambda_o = 610$ nm and $\theta = 70^\circ$. The fluorescence intensity from the Au/PR-hole array substrate increases with the concentration of PSA as shown in Fig. 5a. The fluorescence intensity changes (ΔF) were obtained from the intensity differences of the fitted spectra between the sample and blank (0 ng/ml PSA) at the emission wavelength of 670 nm. The calibration curves in Fig. 5b show that the fluorescence responses on Au/PR-hole substrate are about 2–3 times higher than that on planar Au film, which is in agreement with the enhancement factor of 3 in Fig. 4(b). The limit of detection (LOD) was estimated at 10 and 30 ng/ml for Au/PR-hole array and planar Au film, respectively. The LOD is determined as the concentration of PSA at which the fluorescence intensity changes are three times of the standard deviation of the background signal. The sensitivity is poorer than the conventional surface plasmon-enhanced fluorescence spectroscopy (SPFS) [29], partially because SPFS has a highly sensitive photomultiplier and the low noise level due to the total internal reflection. However, we believe that the fluorescence enhancement on our substructure can be further improved by, for instance, (1) tuning the incident angle to 20° for Au/PR-hole array or using the Au-hole array at an incident angle of 70°, (2) using dark-field fluorescence detection system, (3) combining LSPR with propagating SPR for fluorescence enhancement and (4) selective modification of the nanostructures to allow the molecular binding only on the plasmonic hotspots such as the edges of the nanoholes where the field intensity is at maximum.

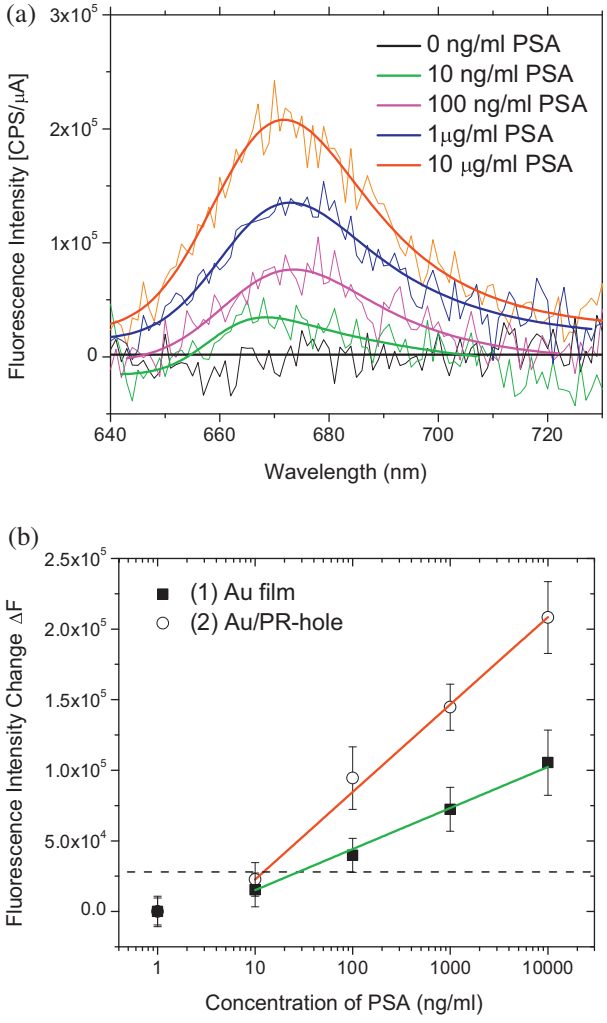

Fig. 5. (a) Fluorescence spectra for the detection of PSA on Au/PR-hole array at the concentrations from 0 to 10 μg/ml in PBST buffer. (b) Calibration curves for the immunoassay carried on a planar Au film and an Au/PR-hole array substrate.

4. Conclusions

We have studied the plasmon wavelength shifts, field distribution and fluorescence enhancements on gold nanohole arrays upon the illumination at various incident angles. The simulations and angular fluorescence measurements demonstrated that the plasmon resonant wavelength and fluorescence enhancement on Au-hole array are less affected by the light incident angles as compared with the Au/PR-hole array. At the excitation wavelength of 610 nm, a fluorescence enhancement up to 14 and 12 can be achieved on Au-hole at the light incident angle of 70° and Au/PR-hole arrays at the angle of 20° with the same pitch of 400 nm and the diameter of 140 nm, respectively. At the incident angle of 70°, a model sandwich assay for the detection of PSA showed that the sensitivity can be improved by 3-fold on Au/PR-hole array as compared with Au film, which is consistent with the fluorescence enhancement measurement. Our research results offer a basic understanding on angular dependence of

fluorescence enhancement, which may help improving design rules for future plasmonic nanostructures on conjunction with dark-field microscopy for highly sensitive fluorescence detection.

Acknowledgements

This research is supported by Science & Engineering Research Council (SERC) of Agency for Science, Technology and Research (A*STAR), for projects under the numbers of 102 152 0014 and 102 152 0015. We are greatly indebted to the SERC nano fabrication, processing and characterization (SnFPC) at the Institute of Materials Research and Engineering (IMRE) for providing the facilities for fabricating the gold nanohole samples.

References

[1] T. Sannomiya, O. Scholder, K. Jefimovs, C. Hafner, A.B. Dahlin, Investigation of plasmon resonances in metal films with nanohole arrays for biosensing applications, Small 7 (2011) 1653–1663.
[2] A.B. Dahlin, M.P. Jonsson, F. Hook, Specific self-assembly of single lipid vesicles in nanoplasmonic apertures in gold, Advanced Materials 20 (2008) 1436.
[3] L. Feuz, P. Jonsson, M.P. Jonsson, F. Hook, Improving the limit of detection of nanoscale sensors by directed binding to high-sensitivity areas, ACS Nano 4 (2010) 2167–2177.
[4] A. Dahlin, M. Zach, T. Rindzevicius, M. Kall, D.S. Sutherland, F. Hook, Localized surface plasmon resonance sensing of lipid-membrane-mediated biorecognition events, Journal of the American Chemical Society 127 (2005) 5043–5048.
[5] H. Im, N.C. Lindquist, A. Lesuffleur, S.H. Oh, Atomic layer deposition of dielectric overlayers for enhancing the optical properties and chemical stability of plasmonic nanoholes, ACS Nano 4 (2010) 947–954.
[6] J.P. Monteiro, L.B. Carneiro, M.M. Rahman, A.G. Brolo, M.J.L. Santos, J. Ferreira, E.M. Girotto, Effect of periodicity on the performance of surface plasmon resonance sensors based on subwavelength nanohole arrays, Sensors and Actuators B: Chemical 178 (2013) 366–370.
[7] M.J. Levene, J. Korlach, S.W. Turner, M. Foquet, H.G. Craighead, W.W. Webb, Zero-mode waveguides for single-molecule analysis at high concentrations, Science 299 (2003) 682–686.
[8] A.G. Brolo, S.C. Kwok, M.G. Moffitt, R. Gordon, J. Riordon, K.L. Kavanagh, Enhanced fluorescence from arrays of nanoholes in a gold film, Journal of the American Chemical Society 127 (2005) 14936–14941.
[9] A.G. Brolo, S.C. Kwok, M.D. Cooper, M.G. Moffitt, C.W. Wang, R. Gordon, J. Riordon, K.L. Kavanagh, Surface plasmon-quantum dot coupling from arrays of nanoholes, Journal of Physical Chemistry B 110 (2006) 8307–8313.
[10] H. Rigneault, J. Capoulade, J. Dintinger, J. Wenger, N. Bonod, E. Popov, T.W. Ebbesen, P.F. Lenne, Enhancement of single-molecule fluorescence detection in subwavelength apertures, Physical Review Letters 95 (2005).
[11] Y.D. Liu, S. Blair, Fluorescence enhancement from an array of subwavelength metal apertures, Optics Letters 28 (2003) 507–509.
[12] Y. Liu, J. Bishop, L. Williams, S. Blair, J. Herron, Biosensing based upon molecular confinement in metallic nanocavity arrays, Nanotechnology 15 (2004) 1368–1374.
[13] P.F. Guo, S. Wu, Q.J. Ren, J. Lu, Z.H. Chen, S.J. Xiao, Y.Y. Zhu, Fluorescence enhancement by surface plasmon polaritons on metallic nanohole arrays, Journal of Physical Chemistry Letters 1 (2010) 315–318.
[14] S. Mayilo, M.A. Kloster, M. Wunderlich, A. Lutich, T.A. Klar, A. Nichtl, K. Kurzinger, F.D. Stefani, J. Feldmann, Long-range fluorescence quenching by gold nanoparticles in a sandwich immunoassay for cardiac troponin T, Nano Letters 9 (2009) 4558–4563.
[15] R. Chhabra, J. Sharma, H.N. Wang, S.L. Zou, S. Lin, H. Yan, S. Lindsay, Y. Liu, Distance-dependent interactions between gold nanoparticles and fluorescent molecules with DNA as tunable spacers, Nanotechnology 20 (2009).
[16] Y. Chen, K. Munechika, D.S. Ginger, Dependence of fluorescence intensity on the spectral overlap between fluorophores and plasmon resonant single silver nanoparticles, Nano Letters 7 (2007) 690–696.
[17] L. Wu, P. Bai, E.P. Li, Designing surface plasmon resonance of subwavelength hole arrays by studying absorption, Journal of the Optical Society of America B 29 (2012) 521–528.
[18] L. Wu, P. Bai, X. Zhou, E.P. Li, Reflection, Transmission modes in nanohole-array-based plasmonic sensors, IEEE Photonics Journal 4 (2012) 26–33.
[19] A. Kinkhabwala, Z.F. Yu, S.H. Fan, Y. Avlasevich, K. Mullen, W.E. Moerner, Large single-molecule fluorescence enhancements produced by a bowtie nanoantenna, Nature Photonics 3 (2009) 654–657.
[20] T. Lohmuller, L. Iversen, M. Schmidt, C. Rhodes, H.L. Tu, W.C. Lin, J.T. Groves, Single molecule tracking on supported membranes with arrays of optical nanoantennas, Nano Letters 12 (2012) 1717–1721.
[21] X.Q. Cui, K. Tawa, K. Kintaka, J. Nishii, Enhanced fluorescence microscopic imaging by plasmonic nanostructures: from a 1D grating to a 2D nanohole array, Advanced Functional Materials 20 (2010) 945–950.
[22] X.Q. Cui, K. Tawa, H. Hori, J. Nishii, Tailored plasmonic gratings for enhanced fluorescence detection and microscopic imaging, Advanced Functional Materials 20 (2010) 546–553.
[23] S.M. Tabakman, L. Lau, J.T. Robinson, J. Price, S.P. Sherlock, H.L. Wang, B. Zhang, Z. Chen, S. Tangsombatvisit, J.A. Jarrell, P.J. Utz, H.J. Dai, Plasmonic substrates for multiplexed protein microarrays with femtomolar sensitivity and broad dynamic range, Nature Communications 2 (2011), http://dx.doi.org/10.1038/Ncomms1477.
[24] F. Hao, E.M. Larsson, T.A. Ali, D.S. Sutherland, P. Nordlander, Shedding light on dark plasmons in gold nanorings, Chemical Physics Letters 458 (2008) 262–266.
[25] E.D. Palik, G. Ghosh, Handbook of Optical Constants of Solids, Academic Press, San Diego, 1998.
[26] T.I. Wong, S. Han, L. Wu, Y. Wang, J. Deng, C.Y.L. Tan, P. Bai, Y.C. Loke, X.D. Yang, M.S. Tse, S.H. Nge, X. Zhou, High throughput and high yield nanofabrication of precisely designed gold nanohole array for fluorescence enhanced detection on biomarkers, Lab Chip 13 (2013) 2405–2413.
[27] C.S. Yun, A. Javier, T. Jennings, M. Fisher, S. Hira, S. Peterson, B. Hopkins, N.O. Reich, G.F. Strouse, Nanometal surface energy transfer in optical rulers, breaking the FRET barrier, Journal of the American Chemical Society 127 (2005) 3115–3119.
[28] M.E. Stewart, N.H. Mack, V. Malyarchuk, J.A.N.T. Soares, T.W. Lee, S.K. Gray, R.G. Nuzzo, J.A. Rogers, Quantitative multispectral biosensing and 1D imaging using quasi-3D plasmonic crystals, Proceedings of the National Academy of Sciences of the United States of America 103 (2006) 17143–17148.
[29] Y. Wang, A. Brunsen, U. Jonas, J. Dostalek, W. Knoll, Prostate specific antigen biosensor based on long range surface plasmon-enhanced fluorescence spectroscopy and dextran hydrogel binding matrix, Analytical Chemistry 81 (2009) 9625–9632.

Biographies

Yi Wang is a research fellow at Center for Biomimetic Sensor Science (CBSS) in Nanyang Technological University, Singapore. He obtained his Ph.D. in 2010 from Max-Planck Institute for Polymer Research in Mainz, Germany. His current research interests include the development of plasmonic nanostructure, novel polymer and peptide-functionalized materials for optical, electrical biosensors.

Lin Wu is a research scientist in Institute of High Performance Computing (IHPC), A-STAR, Singapore. She obtained her Ph.D. in 2009 in Nanyang Technological University, Singapore. Her current research interests include the simulation and modeling of plasmon devices, plasmon-assisted photoelectric effect and ultrafast devices.

Xiaodong Zhou is a senior scientist in IMRE, A-STAR. She obtained her Ph.D. degree in 1995 on information and electronics engineering, and has strong experience in optical and photonic based R&D, electrochemical, surface plasmon resonsnce (SPR), localized surface plasmon resonance (LSPR) based optical bio-NEMS/MEMS devices, and nanoimprinting technology with its related applications on plasmonics and biosensors.

Ten It Wong is a senior specialist in IMRE, A-STAR. He received the M.Sc. in Physics from University Sains Malaysia, 2006. His current interests include nanofabrication, oxides film growth and computational condensed matter.

Jinling Zhang is a Ph.D. student in Nanyang Technological University. She got her bachelor degree at Shanghai Jiao Tong University, China. She currently involves in the development of biosensor based on nanocomposites and surface plasmon resonance.

Ping Bai is a senior scientist in IHPC, A-STAR, Singapore. He has been leading the Plasmonic and Nanointegration Group for the effort of building high-performance devices and systems with synergy of nanophotonics and nanoelectronics. His research has focused on nanoelectronic and optoelectronic devices modeling and the electrical circuit and system design. Currently, he is actively involved in plasmonic and nanophotonic structures that are used for on-chip photonic–electronic integration and plasmonic sensing.

Er Ping Li is the director of Electronics & Photonics Department in IHPC, A-STAR. His research interests include the plasmonics devices, computational electromagnetics and EMC/EMI, nano-scale integrated circuits and their package integration modeling.

Bo Liedberg is currently a full professor of materials science and the director of CBSS, Nanyang Technological University, Singapore. He is also professor at Linköing University, Sweden. Liedberg is heading a research group of about 25 Ph.D. students, postdocs and staff. His basic research is primarily devoted to soft materials science including surface chemistry, self-assembly, supramolecular chemistry and biomimetics. He is also developing new tools for applications in biosensor and medical diagnostics.